Experimental investigation of NO x impact on ignition delay times for lean H 2 /air mixtures using a rapid compression machine under internal combustion engine conditions

N. Villenave, G. Dayma, P. Brequigny, Fabrice Foucher

▶ **To cite this version:**

N. Villenave, G. Dayma, P. Brequigny, Fabrice Foucher. Experimental investigation of NO x impact on ignition delay times for lean H 2 /air mixtures using a rapid compression machine under internal combustion engine conditions. Fuel, 2024, 374, pp.132482. 10.1016/j.fuel.2024.132482 . hal-04648245

HAL Id: hal-04648245
https://hal.science/hal-04648245

Submitted on 15 Jul 2024

HAL is a multi-disciplinary open access archive for the deposit and dissemination of scientific research documents, whether they are published or not. The documents may come from teaching and research institutions in France or abroad, or from public or private research centers.

L'archive ouverte pluridisciplinaire **HAL**, est destinée au dépôt et à la diffusion de documents scientifiques de niveau recherche, publiés ou non, émanant des établissements d'enseignement et de recherche français ou étrangers, des laboratoires publics ou privés.

Distributed under a Creative Commons Attribution 4.0 International License

Fuel 374 (2024) 132482

Contents lists available at ScienceDirect

Fuel

journal homepage: www.elsevier.com/locate/fuel

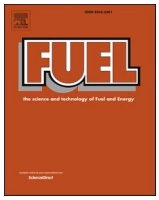

Full Length Article

Experimental investigation of NO_x impact on ignition delay times for lean H_2/air mixtures using a rapid compression machine under internal combustion engine conditions

N. Villenave [a,*], G. Dayma [b,c], P. Brequigny [a], F. Foucher [a]

[a] Univ. Orléans, INSA-CVL, PRISME, EA 4229, F45072 Orléans, France
[b] CNRS ICARE, Avenue de la Recherche Scientifique, 45071 Orléans Cedex 2, France
[c] Université d'Orléans, Orléans Cedex 2, France

ARTICLE INFO

Keywords:
Hydrogen
Nitric oxides
Ignition delay times
Rapid compression machine
Internal combustion engines
Kinetic mechanisms

ABSTRACT

This study investigates the effects of nitric oxides addition on ignition delay times of lean hydrogen/air mixtures ($\varphi = 0.4$), in the 890 K – 1000 K temperature range and for medium-to-high compression pressures ($p_C = 30$, 40, 50, and 60 bar). Results show that ignition delay times decrease with the addition of nitric oxide and nitrogen dioxide, regardless of the compression pressure. These datasets provide new insights to assess the validity of kinetic mechanisms under such conditions and predict autoignition phenomena. As such, a comparison with recent kinetic mechanisms is conducted. A sensitivity analysis on OH radical is performed and highlights the role of the HO_2/H_2O_2 and NO/NO_2 recycling sequences in OH production, yielding an increase in the mixture reactivity. Finally, this work highlighted the importance weight of (R17) in reactivity enhancement and gave a perspective to optimize NO_x sub-mechanisms for hydrogen ignition under internal combustion engine conditions.

1. Introduction

Global warming is a crucial issue in the upcoming years, and the acceleration of the energy transition can no longer be postponed. The European "Net Zero Emission" scenario consists in the entire replacement of fossil fuels by renewable energy and free-carbon devices to limit the increase up to 1.5 °C by 2050 [1,2]. The transport sector is the second most polluting sector with emissions of around 7000 Mt of CO_2 in 2020 [3]. The key to decarbonizing this industry is replacing hydrocarbons such as diesel and gasoline with promising green e-fuels such as hydrogen (H_2). Hydrogen internal combustion engines (H_2ICEs) are a way to drastically reduce greenhouse gas emissions, especially if H_2 is produced through water electrolysis and/or photochemical water-splitting instead of methane steam-reforming [4]. Moreover, H_2ICEs are attractive because they allow an increase in thermal efficiency in comparison to hydrocarbon-fueled ICEs [5]. As a matter of fact, in comparison to hydrocarbon fuels, H_2 combustion properties, presented in Table 1, are promising, and its use as a fuel offers many advantages [6]. For example, the laminar flame speed of H_2 (~2.4 m/s) is almost five times higher than that of gasoline (C_8H_{18}) (~0.4 m/s) at the stoichiometry ($\varphi = 1$), ambient temperature and standard pressure. This difference partly explains the higher efficiency of H_2ICEs, attributed to its faster combustion speed and wide range of flammability. However, such flame properties also brings disadvantages, especially for internal combustion engines where almost all abnormal combustion phenomenon are attributed to both properties.

It is important to emphasize that the concept of H_2ICE is hardly a new development. Das et al. [7] presented an overview of the development of H_2ICEs since 1930. This study highlights various undesirable combustion phenomena due to the physico-chemical properties of H_2 such as backfire, pre-ignition, and knocking. For the sake of clarity, backfire is a phenomenon induced by the interaction between the inlet H_2/air mixture with a source of high thermal energy to start combustion while the intake valves are still open. Pre-ignition occurs when the H_2/air mixture ignites before the spark timing while knocks are close to the pre-ignition problems caused by hot spots created far from the valve in the combustion chamber. Furthermore, the H_2 flame temperature is high (~2400 K at $\varphi = 1$), prone to high pollutant emissions especially nitric oxides (NO, NO_2) through the thermal-NO formation path, in addition to prompt-NO and N_2O routes [8]. For all these reasons, recent studies, presented in [9], agreed on the use of ultra-lean ($\varphi < 0.4$) H_2/air combustion combined with exhaust gas recirculation devices, in H_2 spark-

* Corresponding author at: Univ. Orléans, INSA-CVL, PRISME, EA 4229, F45072 Orléans, France.
E-mail address: nicolas.villenave@univ-orleans.fr (N. Villenave).

https://doi.org/10.1016/j.fuel.2024.132482
Received 17 April 2024; Received in revised form 27 June 2024; Accepted 8 July 2024
0016-2361/© 2024 The Author(s). Published by Elsevier Ltd. This is an open access article under the CC BY license (http://creativecommons.org/licenses/by/4.0/).

Table 1
Hydrogen/air, *iso*-octane/air, methanol/air, and methane/air properties at $T = 298$ K and $p = 1$ bar.

	Hydrogen	Gasoline	Methanol	Methane
Formula	H_2	C_8H_{18}	CH_3OH	CH_4
Density (kg/m^3)	0.08	692	0.791	0.716
Flammability range (φ)	0.2 – 7	0.7 – 4	0.5 – 4.0	0.5 – 1.7
Low Heating Value (MJ/kg)	120	44.3	23	55.5
	Hydrogen/ Air At $T = 298$ K, $p = 1$ bar, $\varphi = 1.0$	Gasoline/ Air At $T = 298$ K, $p = 1$ bar, $\varphi = 1.0$	Methanol/ Air At $T = 298$ K, $p = 1$ bar, $\varphi = 1.0$	Methane/ Air At $T = 298$ K, $p = 1$ bar, $\varphi = 1.0$
Auto-ignition Temperature (K)	860	680	632	506
Adiabatic Temperature (K)	2380	2275	2150	2226
Laminar Flame Speed (m/s)	2.4	0.4	0.43	0.48

ignition engines (H_2SIEs), to avoid undesirable combustion phenomena such as the so-called "super-knocking", while mitigating NO and NO_2 emissions.

Exhaust gas recirculation (EGR) is a promising strategy due to its high-dilution and low-temperature characteristics, promoting species distribution and temperature homogeneity, and thus mitigating NO_x production inside the combustion chamber. The effect of water injection *via* EGR on NO_x emission and combustion parameters of a H_2SIE has been studied and shows an important reduction in NO levels, an increase in the ignition delay, and combustion duration, but no change in cyclic variations under lean conditions [10]. Although water injection has shown great capacity to improve thermal efficiency and NO_x emissions in SIE, some challenges remain: water injection control, water supply systems, water wall wetting, and water injection impact on engine aging [11]. Exhaust gas recirculation (EGR) can be used in both Compression Ignition Engines (CIEs) and SIEs to mitigate NO_x emissions. Indeed, using EGR will reduce the combustion temperature inhibiting NO_x formation. Dhyani et al. [12] performed an experimental study on the EGR effect in a constant-speed multi-cylinder SIE fuelled with H_2, under stoichiometric conditions, to control combustion anomalies as backfire or knocking and reduce NO_x emissions. The EGR rate varied from 0 % to 28 % by volume at a 15 kW load. EGR reduces backfire phenomena and their propagation by a dilution effect and a reduction in flame speed. NO_x emissions decrease when EGR increases. At a high EGR rate, issues with the stability of the combustion process were observed. However, for 25 % EGR, results show a diminution of 57 % for NO_x emissions. The same results were obtained by Nande et al. [13]. EGR was considered as a method for the reduction of knocking and NO_x emissions for stoichiometric operations. Experiments were carried out on a single-cylinder CFR engine at 900 rpm under part-load operation with 410 kPa Net Indicated Mean Effective Pressure, $\varphi = 1$, three different compression ratios (8:1, 10:1, and 12:1), and for various spark timings. Results show that low levels of EGR imply longer combustion duration, and reduction of knock intensities. NO_x emissions decrease from 2500, 3250, and 4250 ppm (respectively to the compression ratio) for 0 % EGR to almost 0 at 35 % EGR regardless of the compression ratio. Hence, the use of EGR in H_2SIEs is a good way to find a trade-off between lean engine condition performance and low NO_x emissions. Nevertheless, it has been shown that the species in EGR may impact the combustion in different ways [14,15], especially if a long-route or a short-route EGR loop (after or before the catalyst respectively) is used, NO and NO_2 are present in the air-EGR mixture at the intake.

A key to understand the impact of NO_x on hydrogen combustion is the study of H_2/Air/NO_x autoignition characteristics under ICE conditions. The use of a rapid compression machine (RCM) facility enables to reach high-pressure and low-temperature conditions in the "weakly explosive" zone, as illustrated in Fig. 1, which are very close to relevant engine conditions. Several studies have been conducted on the impact of NO_x on hydrocarbons ignition delays using a RCM and mimicking ICE conditions (650 K < T < 1000 K, 15 bar < p < 100 bar) [16–22]. These work highlights the non-linear impact of NO_x addition on mixtures reactivity and draws attention on the accuracy of the chemical models.

According to the best of the author's knowledge, few recent studies report the impact of NO_x on H_2/O_2/diluent ignition delay times, particularly under H_2SIEs conditions. This topic was first investigated by Slack and Grillo [23] measuring the impact of NO and NO_2 on induction times for stoichiometric H_2/air mixtures at $p = 0.27 – 3.0$ atm, $T = 800 – 1500$ K, using a shock tube. A wide range of mixture compositions were studied: $X_{NO} = 0$, 0.5, 1, 2.25, 4.5; $X_{NO2} = 0.75$, 1.50, 3.56; $X_{NO}/X_{NO2} = 1.1/0.85$. General observation shows that NO_x reduces significantly induction times. Later, the impact of NO_2 on H_2/O_2/Ar mixtures was studied by Mathieu et al. [24] also using shock tubes in a comprehensive modeling study. The study was performed for different NO_2 mole fractions (100, 400, and 1600 ppm), different φ for 100 ppm of NO_2 (0.3, 0.5, 1), and different pressure conditions (1.5, 13, and 30 atm). It shows an important dependence of ignition delays on the pressure and the NO_2 concentration in contrast to equivalence ratio variation. Regarding relevant H_2SIEs conditions ($p = 30$ atm), the addition of NO_2 enhances H_2/air mixture reactivity and reduces IDT, especially for the "lower" temperature conditions (~1050 K).

In light of these studies, it is crucial to study the impact of NO_x on lean H_2/air ignition delays under SIE conditions. Noteworthily, to the best of the author's knowledge, ignition delays of lean H_2/Air/NO_x mixtures for low-to-intermediate temperature and medium-to-high pressure have never been investigated using a RCM. Therefore, the present work focuses on ignition delays measurement from lean H_2/Air/NO_x mixtures on a RCM for a pressure range of 30 bar up to 60 bar, a temperature range of 890 K to 1000 K, and for NO_x concentration variations from 50 ppm to 1250 ppm. Numerical simulations were performed to validate kinetic mechanisms and interpret the present results. Finally, sensitivity analyses were carried out for different NO_x quantities and pressures to highlight the reactions involved in the mixture reactivity.

2. Experimental and numerical methodology

2.1. Experimental setup and ignition delay times measurement

The experimental facility used in this study is a rapid compression

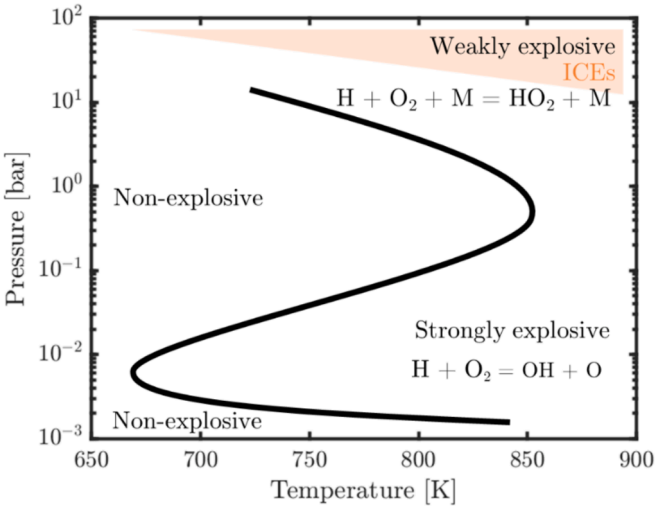

Fig. 1. Explosion limits of H_2/O_2 mixtures at $\varphi = 1.0$.

machine (RCM) designed at Orléans University. The RCM is illustrated in Fig. 2 and a detailed description of the RCM and its operating conditions can be found in [25]. The RCM is equipped with a single piston, pneumatically driven and hydraulically stopped at the end of the compression to reach the desired thermodynamic conditions at the top dead-center position. The piston used in this work has been designed with a crevice head to prevent vortex roll-up formation and ensure the homogeneity of the core gas [26]. This homogeneity allows the use of the adiabatic core hypothesis to calculate the conditions at the top dead center in the cylinder (see Section 2.2). The intake temperature (T_0) was measured with a K-thermocouple type with an uncertainty of ± 1 K. The intake pressure in the cylinder (p_0) and the pressure at the end of the compression (p_C) were measured with a pressure sensor KELLER PAA-33X/80794 (with an accuracy of 0.05 % FS over a range of 0 – 5 bar, corresponding to an uncertainty of 2.5 mbar) and with a piezoresistive transducer AVL QH32C (linearity of ± 0.2 % and accuracy of ± 1 %), respectively. The different H_2/Air/NO_x mixtures studied here were prepared before the experiments in a stirred tank. The purity of the gases might influence the temperature-dependent specific heat ratio. As such, here is the uncertainty regarding the composition of each gas bottle (H_2: 99.993 %, O_2: 99.997 % and N_2: 99.986 %). The pressure sensor used on the reservoir is a KELLER PAA-21Y with an accuracy of 0.5 % FS over a range of 0 – 10 bar, corresponding to an uncertainty of 0.05 bar. This tank is filled with a mass flow controller BROOKS Cori-Flow M13V101 with an accuracy of ± 1 % on the flow rate.

The final temperature is deduced from the adiabatic core hypothesis as follows in Equation (1):

$$\int_{T_0}^{T_C} \frac{\gamma}{\gamma - 1} \frac{dT}{T} = \int_{p_0}^{p_C} \frac{dp}{p} \tag{1}$$

where p_0, T_0, p_C, T_C, and γ are respectively the intake pressure, the intake temperature, the compression pressure, the compression temperature, and the temperature-dependent specific heat ratio. As shown in Fig. 3, IDT is determined from the experimental pressure trace and it is defined as the time between the TDC and the first-order time derivative of pressure.

Ignition delay times have been measured for both H_2/O_2/N_2 and H_2/O_2/N_2/NO_x mixtures. These measurements were performed for lean conditions (φ = 0.4), low-to-intermediate temperature, and intermediate-to-high pressure as displayed in Table 2. At least three consecutive shots were recorded for each experimental condition to ensure repeatability and are plotted on the figures. Ignition delays statistical errors were determined using the Moffat methodology [27]. Additional uncertainty in ignition delay measurements also depends on the system acquisition frequency, which is equal to 10 kHz. Thus, the uncertainty on ignition delays is ± 0.1 ms, which is quite negligible. The uncertainties in compression temperatures were assessed following the approach detailed in the modeling study by Baigmohammadi et al. [28]. This assessment considered the purity of the gases, the pressure sensor of the tank vessel, the K-type thermocouple, the pressure sensor used for filling the combustion chamber, and also the piezoresistive pressure transducer used to measure the pressure evolution during the compression. To conclude, the temperature uncertainty at the end of compression is approximately ± 0.5 % (± 4 – 6 K). The focus was made on these operating points because it is of interest in the case of H_2-fuelled SI engines with and without EGR. Both reactive and non-reactive mixtures were studied. Pressure profiles from non-reactive cases were measured in order to represent heat losses in the simulations.

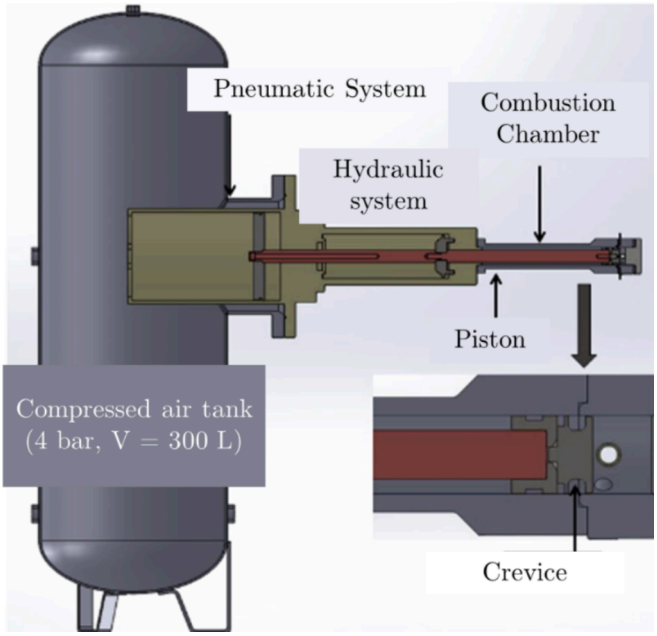

Fig. 2. Rapid compression machine (RCM) from Orléans University.

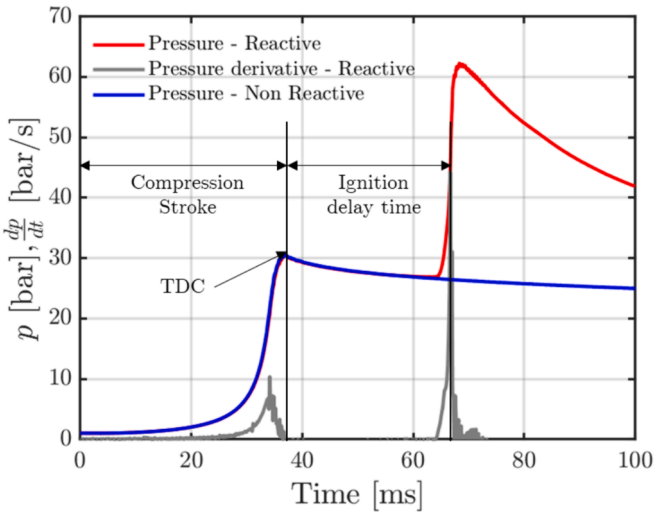

Fig. 3. Experimental pressure profiles from the reactive and the non-reactive case. The reactive case was performed with H_2/O_2/N_2 mixture φ = 0.4, T_C = 957 K, and p_C = 30 bar. The non-reactive case was obtained by replacing O_2 with N_2 in the tank vessel to reach the same thermodynamic conditions as the reactive case.

2.2. Numerical methodology

Closed-homogeneous reactor simulations were performed using the simulation code CHEMKIN PRO [29] to test the capabilities of the recent

Table 2
RCM main characteristics for different experiments. The compression ratio (CR) corresponds to the volume ratio of the combustion chamber at the bottom dead centre configuration and at the top dead centre configuration respectively. T_0 and p_0 are the intake temperature and the intake pressure imposed respectively. p_C is the compression pressure range measured and T_C is the compression temperature obtained after the compression and calculated with the adiabatic core hypothesis.

Parameters	Values
CR [-]	13.2
Piston diameter [mm]	50
T_0 [K]	353 – 393
p_0 [bar]	0.890 – 1.965
T_C [K]	890 – 970
p_C [bar]	30/40/50/60

kinetic mechanisms for $H_2/O_2/N_2$ and $H_2/O_2/N_2/NO_x$ mixtures at low-to-intermediate temperature and medium-to-high pressure conditions. As such, effective adiabatic core volume was implemented using the non-reactive pressure trace to simulate accurately the isentropic compression and therefore account for heat losses before the ignition. Experimental results were compared with different kinetic mechanisms. An exhaustive list of kinetic mechanisms for hydrogen chemistry already exists [30], enabling IDTs prediction with varying degrees of accuracy, for lean H_2/air mixtures, under SIEs conditions. Three recent kinetic mechanisms, in alignment with the targeted conditions, were appraised and their range of validation are detailed in Table 3. In a previous study, Villenave et al. [31] proposed a kinetic mechanism for lean H_2/air mixtures, validated through a comparison with ignition delay measurements, conducted using a RCM at $T_C = 890$ K – 1000 K, $p_C = 20 – 60$ bar and $\varphi = 0.2 – 0.5$. This mechanism is based on the initial mechanism of Burke et al. [32] modified according to Klippenstein et al. [33] study with the addition of the self-reaction $2HO_2 = 2\ OH + O_2$. This kinetic mechanism has demonstrated excellent performance for hydrogen combustion. Simulations using this kinetic mechanism, to which an optimized NO_x sub-mechanism from Glarborg et al. [34] was added, were performed. Furthermore, a comparison will be carried out with two optimized fuel/NO_x kinetic mechanisms: the recently modified detailed kinetic mechanism NUIGMech1.2, proposed by Aljohani et al. [35], and the recent mechanism for $H_2/CO/NO_x$ chemistry proposed by Sun et al. [36]. A comparison will be also made with the GRI-Mech 3.0 mechanism [37], as it remains one of the most widely used kinetic mechanisms in the CFD community, although not designed to model hydrogen combustion. Additionally, it would be valuable to discuss the differences in the NO_x sub-mechanism used by studied kinetic mechanisms. The kinetic mechanism from Aljohani et al. [35] incorporates the NOx sub-mechanism from Glarborg et al. [34]. Noteworthily, this model provides reasonable predictions of the formation and destruction of NO species while considering the significance of $HONO/HNO_2$ decomposition. The NO_x sub-mechanism proposed by Sun et al. [36] is based on many constant rate reaction modifications using high-level quantum chemistry calculations and simulations to address the challenges in reproducing the kinetic decomposition of HONO and HNO_2 under high-pressure conditions. The NO_x sub-chemistry is also presented in the GRI-Mech 3.0 [37] mechanism, but it is not optimized as it only considers the formation and the reburn chemistry of NO.

Table 3
Kinetic mechanisms and experimental conditions for $H_2/O_2/N_2/NO_x$ and fuel/$O_2/N_2/NO_x$ ignition delay times validation.

Kinetic mechanisms	Experimental validation	Mixture	φ	p	T
Villenave et al. [31]	Rapid Compression Machine	$H_2/O_2/N_2$ $X_{N2}/X_{O2} = 3.76$	0.2 – 0.5	20 – 60 bar	870 – 1000 K
Aljohani et al. [35]	Rapid Compression Machine and Shock Tubes	Oxygenated Gasoline (Euro6 E10)/ EGR/$NO_x/O_2/N_2$ EGR: CO_2, H_2O, N_2 $X_{NOx} = 0$, 874, 1501, 3174, 5568 ppm	0.5 – 1.0	20 – 30 bar	658 – 1598 K
Sun et al. [36]	Shock tubes	$H_2/O_2/NO_2/Ar$, $X_{NO2} = 100$, 400, 1600 ppm H_2/Air/NO, $X_{NO} = 0.5$ %	0.3 – 1.01.0	1.5 – 30 atm 2.0 atm	1038 – 1744 K 770 – 1190 K
GRI-Mech 3.0 [37]	Shock Tubes	$CH_4/O_2/NO/Ar$	1.0, 1.6	10 torr, 1.8 bar	2800 K

2.3. NO-NO_2 interconversion

A separate tank is used to prepare the different mixtures and ensure their homogeneity. Initial NO is diluted in a bottle of N_2 and injected into the tank after the reactants. Many studies highlight the fast interconversion of NO into NO_2 in the presence of O_2 through the termolecular reaction $2NO + O_2 = 2\ NO_2$ [38,39]. Typically, modelling a perfectly homogeneous closed reactor enables quantifying this decomposition with optimized rate constants suggested in NO_x sub-mechanisms, as underlined by Aljohani et al [35]. However, in order to quantify more accurately the final mixture composition, prior to its introduction into the combustion chamber, the NO interconversion was measured. Once the filling process is complete, a continuous flow of the prepared mixture is pumped through a precalibrated multi-compo laser infrared spectrometer LaserCEM ®. The measurement uncertainty for NO and NO_2 is ± 5 ppm and to ensure reproducibility, the experiment was repeated three times. Notably, for an initial concentration of $X_{NO,0} = 50$ ppm, the uncertainty at the end of the phase conversion is significant. However, for each repetitions, results did not vary by more than ± 1 ppm. As such, the NO mole fraction, X_{NO}, and NO_2 mole fraction, X_{NO2}, evolutions were recorded, simultaneously for more than thirty minutes. Fig. 4 illustrates the interconversion of NO into NO_2 at $p = 5$ bar and $T = 333$ K, for the targeted initial NO mole fractions: (a) $X_{NO,0} = 50$ ppm, (b) $X_{NO,\ 0} = 250$ ppm, and (c) $X_{NO,0} = 1250$ ppm. First, regardless of $X_{NO,0}$, $X_{NO,}$ and X_{NO2}, profiles display a logarithmic decay and growth, respectively, before reaching a plateau corresponding to the chemical equilibrium. Note that the time required to achieve this equilibrium seems to decrease when $X_{NO,\ 0}$ increases. Three phases are observable: Phase I corresponds to the time interval during which the experimental rig does not allow for a precise determination of X_{NO} and X_{NO2}. Indeed, the mixture is not yet complete, and the reaction between NO and O_2 has already started. Phase II constitutes the measurement range for the interconversion of NO into NO_2. Finally, phase III marks the end of measurements and the time after which the mixture is introduced into the combustion chamber, where it is assumed that the composition of NO and NO_2 remains constant. To validate the reliability of laser detection, the NO phase conversion was also calculated numerically using the studied kinetic mechanisms incorporating relevant NO_x sub-chemistry. The present model demonstrates excellent agreement in NO interconversion for the case where $X_{NO,0} = 50$ ppm. As $X_{NO,0}$ increases, the model seems to predict a faster NO phase conversion, particularly during the transition from region I to region II. Noteworthily, the plateau is well established after thirty minutes of residence time. The kinetic mechanism from Aljohani et al. [35] predicts a slightly faster interconversion compared to the current model, although both exhibit very similar trends. Their good agreement is primarily due to both mechanisms incorporating NO_x sub-chemistry from Glarborg et al. [34]. The NO interconversion was also calculated using the model from Sun et al. [36], which employs a different NO_x sub-mechanism. This model predicts a significantly faster NO interconversion compared to other models and experiments, regardless of $X_{NO,0}$. This discrepancy is potentially due to the consideration of HNO_2 influence on the NO interconversion into NO_2, which is not considered in the NO_x sub-chemistry from Glarborg et al. [34].

Hence, in the light of this study, the X_{NO} and X_{NO2} measured at $t = 2100$ s (35 min) of analysis correspond to X_{NO} and X_{NO2} introduced in the RCM. The compositions of the studied mixtures are summarized in Table 4.

3. Results and discussion

Despite the increasing focus on using EGR devices in H_2SIEs, a crucial lack exists in understanding the impact of EGR on lean H_2/air ignition. While the primary role of EGR is to cool down the flame through mostly

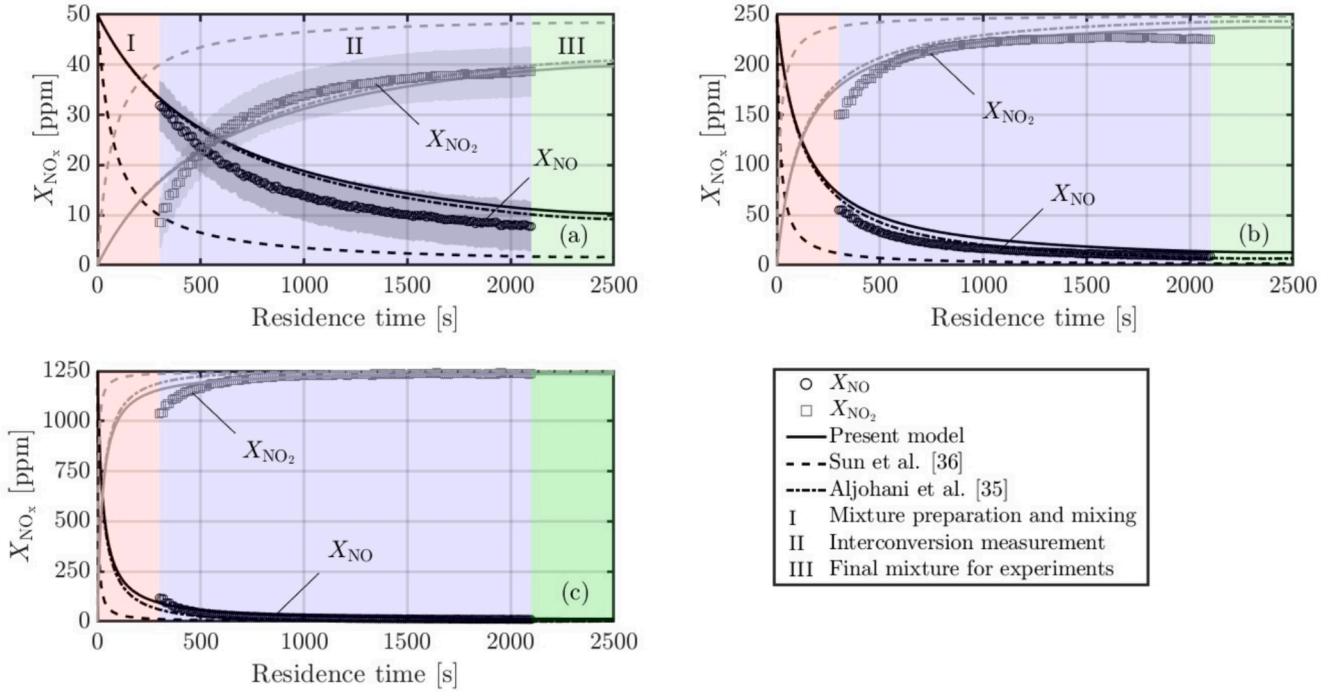

Fig. 4. Comparison of NO and NO_2 mole fractions evolution during the mixing in the RCM tank vessel at $p = 5$ bar, $T = 333$ K. The interconversion of NO into NO_2 was measured and estimated numerically [35,36] for different initial NO mole fractions: (a) $X_{NO,0} = 50$ ppm, (b) $X_{NO,0} = 250$ ppm, and (c) $X_{NO,0} = 1250$ ppm. The residence time corresponds to the time before RCM experiments.

Table 4
$H_2/O_2/N_2$ and $H_2/O_2/N_2/NO_x$ mixtures for the experiments introduced in a 4.18 L tank vessel at 333 K. Mixture #1: Pure H_2/air, mixture #2: $X_{NO,0} = 50$ ppm, mixture #3: $X_{NO,0} = 250$ ppm, mixture #4: $X_{NO,0} = 1250$ ppm.

#	φ	H_2 [% mol]	O_2 [% mol]	N_2 [% mol]	X_{NO} [ppm]	X_{NO2} [ppm]
1	0.4	14.38	17.98	67.64	0	0
2	0.4	14.38	17.98	67.64	8	42
3	0.4	14.38	17.98	67.64	9	241
4	0.4	14.38	17.98	67.64	11	1239

N_2 dilution, other species such as NO_x and even H_2O may have a substantial impact on the mixture reactivity. Fig. 5 illustrates the impact of NO_x addition on H_2/air IDTs under lean conditions ($\varphi = 0.4$) and for moderate-to-high compression pressures p_C = (a) 30, (b) 40, (c) 50, (d) 60 bar.

It may first be noted that ignition delay times show excellent repeatability, and none of these experimental data points seem to suffer from pre-ignition. As mentioned in *Section 3*, the fuel and oxidizer mixtures were fully premixed using a constantly stirred-fan tank. The short time interval between filling the combustion chamber and compression allows very short time for the mixture to develop inhomogeneities. Additionally, the accurate control of initial temperature, initial pressure, and crevice design enables repeatable experiments, minimizing variations in ignition delays. On the one hand, for a fixed mixture composition, ignition delay time decreases with the increase of the compression pressure, as already observed for pure hydrogen [31]. On the other hand, regardless of p_C, ignition delay times depict a decrease with the increase of X_{NOx}. At low pressure ($p_C = 30$ bar) and $T_C = 920$ K, a NO_x addition of 50 ppm reduces the ignition delay by 18 %. However, for $X_{NOx} = 250$ ppm and $X_{NOx} = 1250$ ppm, ignition delays are drastically reduced by 50 % and 92 %, respectively. Conversely, at $T_C = 980$ K, a NO_x addition of 50 ppm and 250 ppm decreases the ignition delay by 11 % and 36 %, respectively, while for $X_{NOx} = 1250$ ppm, IDTs are too short to be measured (<1 ms). As such, ignition delays appear to be more sensitive to NO_x addition at lower temperatures within the specified pressure range. These observations are applicable for both $p_C = 40$ bar and $p_C = 50$ bar. At a higher compression pressure ($p_C = 60$ bar) and the lowest temperature condition ($T_C = 900$ K), the introduction of 50 ppm of NO_x results in a moderate 12 % reduction in the ignition delay. However, for $X_{NOx} = 250$ ppm and $X_{NOx} = 1250$ ppm, IDTs are drastically reduced by 46 % and 88 %, respectively. Interestingly, the promoting effect of NO_x seems to decrease as p_C increases; however, this experimental trend falls within the range of uncertainty of the measurements.

Overall, these new experimental results demonstrate that NO_x addition enhances the reactivity of lean H_2/air mixtures. The fact that small amounts of NO_x can significantly impact ignition delays is of primary importance for the design and optimization of H_2ICEs. Indeed, the lower the ignition delays, the more likely H_2SIE is prone to knocking (after spark ignition) and/or super-knocking (before spark ignition) [40]. Prevent knocking and super-knocking, through 0-D or 1-D numerical simulation, as an initial step for three-dimensional (3-D) H_2SIE simulations, is not an unexplored concept. Li and Karim [41] already proposed a two-zone numerical model able to predict knocking in hydrogen engines while Ye et al. [42] and Li et al. [43] proposed a 3-D numerical approach for H_2SIEs. As such, these numerical studies underline the crucial need for comprehensive and relevant kinetic mechanisms, able to predict the impact of NO_x on H_2/air ignition delay times. In light of these studies, three H_2/air/NO_x kinetic mechanisms (see *Section 3*) were appraised. For each reactive pressure profile, a non-reactive one is associated, and simulated ignition delays account for heat losses.

The relative difference in ignition delay time (ϵ) is presented in Equation (2) and is calculated to determine the agreement between the experimental and the simulated ignition delays (τ^{exp} and τ^{sim}, respectively).

$$\epsilon = \frac{(\tau^{sim} - \tau^{exp})}{\tau^{exp}} \cdot 100 \quad (2)$$

All mean relative deviations ($\bar{\epsilon}$) were calculated and are presented in

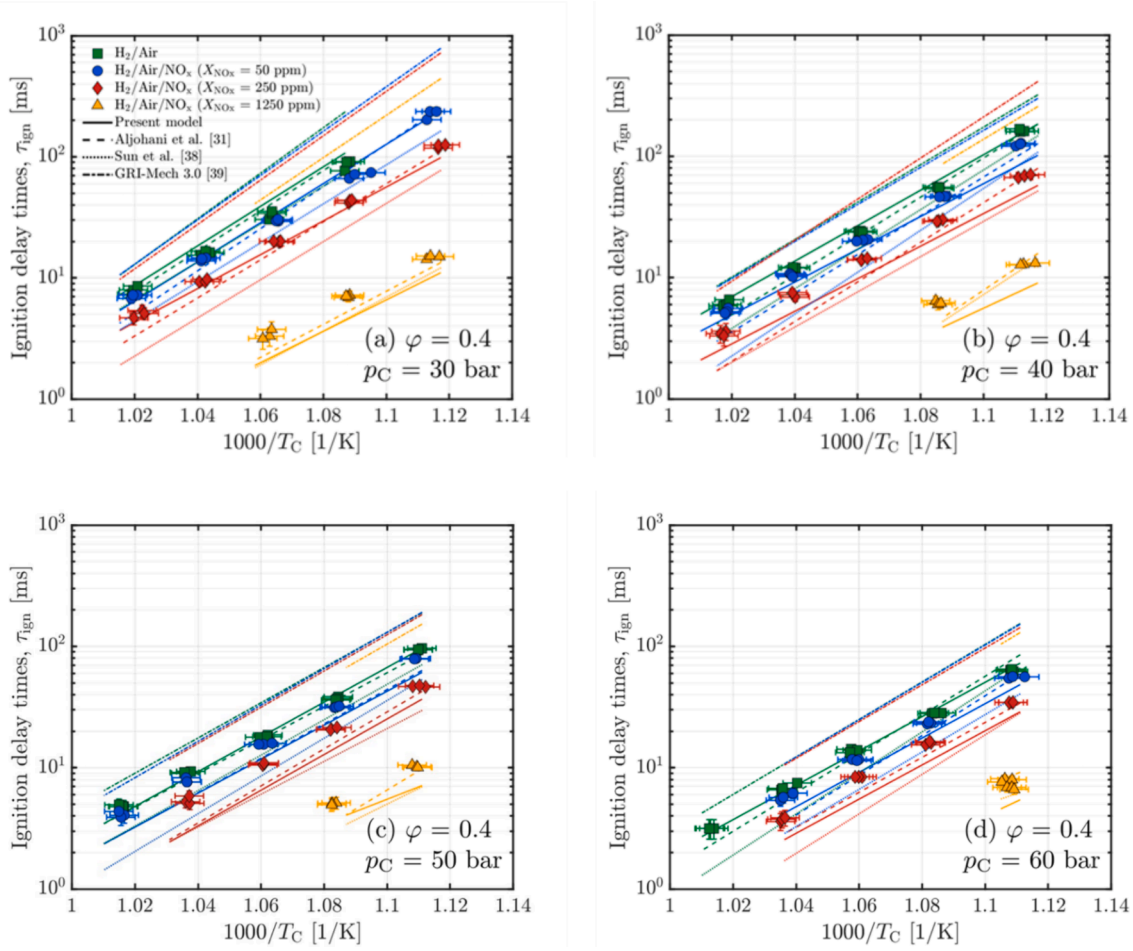

Fig. 5. Ignition delays times of $H_2/O_2/N_2/NO_x$ mixtures at φ = 0.4, p_C = 30 (a), 40 (b), 50 (c), 60 (d) bar and for different NO_x mole fractions: X_{NOx} = 0 ppm, 50 ppm, 250 ppm and 1250 ppm. Comparison with the present model, Aljohani et al. model [35], Sun et al. model [36], and the GRI-Mech 3.0 model [37].

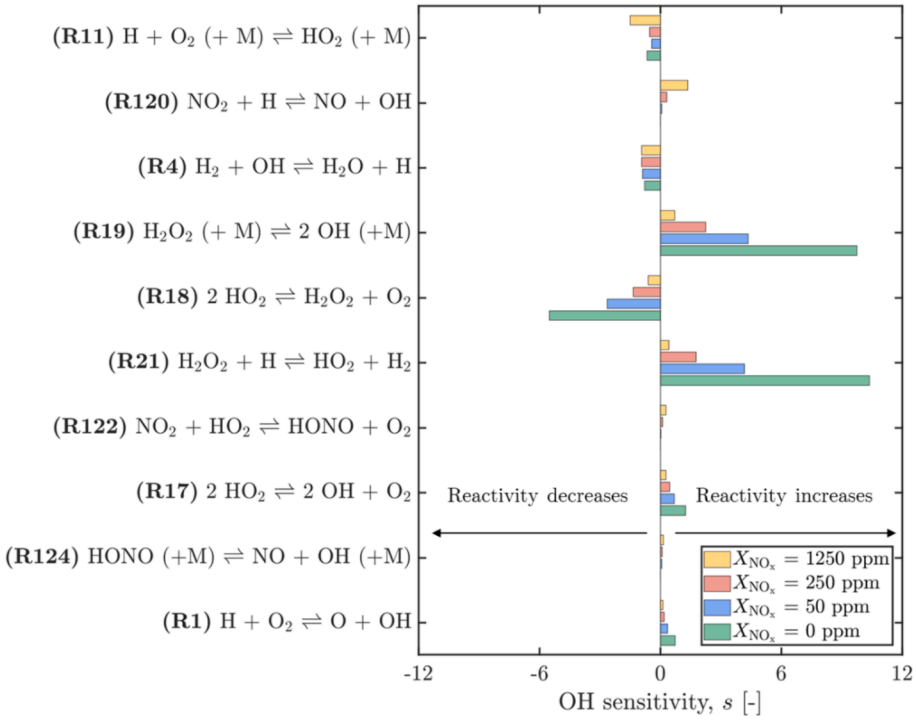

Fig. 6. Sensitive reactions on OH radical for H_2/air/NO_x mixtures for X_{NOx} = 0 ppm, 50 ppm, 250 ppm, 1250 ppm at p_C = 50 bar, and T_C = 908 K.

the Supplementary Materials. Globally, the calculated ignition delay times obtained from the model developed in this work show the best agreement with our experimental results. Indeed, the present model exhibits the best-bounded absolute relative difference, ranging from $\epsilon = 0.6$ % at $p_C = 30$ bar and $T_C = 920$ K for a pure H_2/air mixture up to $\epsilon = 47.8$ % at $p_C = 60$ bar and $T_C = 960$ K. Noteworthily, this model tends to underpredict ignition delays as X_{NOx} increases, especially at higher pressures, averaging a $\epsilon = 40$ % relative deviation. The Aljohani et al. mechanism demonstrates similar good performance under all the targeted conditions, being slightly too reactive for the highest temperatures, but exhibiting a better agreement for the lowest temperatures. The mechanism proposed by Sun et al. exhibits more discrepancies, being too reactive when X_{NOx} increases, with a relative difference ranging from $\epsilon = -20$ % at $p_C = 30$ bar and $T_C = 920$ K to $\epsilon = -73.3$ % at $p_C = 60$ bar and $T_C = 960$ K. Finally, the GRI-Mech 3.0 model fails to accurately predict ignition delays for pure H_2/air mixtures, with a minimum absolute relative difference of 50 %. Additionally, it appears that this mechanism does not capture $H_2/O_2/NO_x$ chemistry as well. It consistently overpredicts ignition delay times for all the studied conditions and seems insensitive to NO_x addition, while it is still widely used. Consequently, the current model constitutes a promising candidate for predicting ignition delay times in lean H_2/air/NO_x mixtures under internal combustion engine conditions.

A sensitivity analysis on OH radical regarding X_{NOx} addition is illustrated in Fig. 6. This analysis was performed using the present model, at 5 % of H_2 consumption, $T_C = 908$ K, $p_C = 50$ bar, and for $X_{NOx} = 0$, 50, 250, 1250 ppm. An identical sensitivity analysis on OH radical was conducted for the kinetic mechanism from Aljohani et al. [35], which shows very good performance, particularly under conditions with the highest NO_x concentrations. This sensitivity analysis is available in the Supplementary Materials. Only the ten most sensitive reactions are presented and note that the most sensitive reactions are always the same except for the case with pure H_2. Concerning pure H_2/air mixtures, there is a well-known competition between the two most promoting reactions (R19) H_2O_2 (+M) = 2 OH (+M) ($s_{R19} = 9.8$), (R21) $H_2O_2 + H = HO_2 + H_2$ ($s_{R21} = 10.4$) and the most inhibiting reaction (R18) 2 $HO_2 = H_2O_2 + O_2$ ($s_{R18} = -5.53$). The sensitivity of these reactions decreases when X_{NOx} increases while (R4) $H_2 + OH = H_2O + H$ sensitivity remains globally constant, with $-0.8 < s_{R4} < -0.9$. When X_{NOx} increases, the third-body chain terminating reaction (R11) becomes one of the most sensitive reactions, decreasing the reactivity of the mixture by consuming H radicals to produce more stable HO_2 radicals. However, as the experiments are conducted on the weakly explosive side, HO_2 reacts with H_2 through the chain continuation reaction (R21) $HO_2 + H_2 = H + H_2O_2$ ($s_{R21} = 0.4$ when $X_{NOx} = 1250$ ppm) to produce H atoms and hydrogen peroxide, H_2O_2. Under these conditions, H_2O_2 is not stable and it breaks into two OH via the third-body chain branching reaction (R19) H_2O_2 (+M) = 2 OH (+M) ($s_{R19} = 0.29$ when $X_{NOx} = 1250$ ppm), increasing the reactivity of the mixture. This highlights that a portion of OH radicals is produced through HO_2/H_2O_2 sequences, albeit the sensitivity decreases with increasing X_{NOx}. Alongside, the inhibiting reactions (R11) and (R4) competes with NO/NO_2 reactions (R120) $NO_2 + H = NO + OH$, (R122) $NO_2 + HO_2 = HONO + O_2$ and (R124) HONO (+M) = NO + OH (+M), as X_{NOx} increases. Noteworthily, the sensitivity of these reactions is always positive, indicating reactivity enhancement. For $X_{NOx} = 50$ ppm and $X_{NOx} = 250$ ppm, the aforementioned reaction sensitivities are very low, explaining the slight impact of NO_x on ignition delay times. However, for $X_{NOx} = 1250$ ppm, (R120) becomes the most sensitive reaction on the "promoting" side ($s_{R120} = 1.4$), illustrating the impact of NO_x on the reactivity enhancement. As observed in Fig. 4, the mixture is mostly composed of NO_2, and during the induction time, it reacts directly with H to create NO and OH *via* (R120). In the meantime, NO interacts with HO_2 through (R118) $NO + HO_2 = NO_2 + OH$ and regenerates NO_2. This is underlined by numerical simulations, presented in the Supplementary Materials, which give similar results when considering that NO_x is composed only of NO or NO_2. There is another path for NO_2 consumption through the chain reactions (R122) $NO_2 + HO_2 = HONO + O_2$ ($s_{R122} = 0.26$) and (R125) $NO_2 + H_2 = HONO + H$, both producing nitrous acid HONO, which could constitute a well for OH. Nevertheless, under the targeted pressure conditions (30 bar $< p <$ 60 bar), the decomposition of nitrous acid is favored through reaction (R124) HONO (+M) = NO + OH (+M) ($s_{R124} = 0.15$), increasing also the reactivity. As such, the HO_2/H_2O_2 sequence is not the exclusive contributor to OH production; indeed, there is a recycling loop between NO and NO_2 contributing to a more important production of OH, promoting of the overall reactivity of the mixture and thus decreasing ignition delay times.

Discrepancies between experimental results and IDTs calculated with thepresent mechanism are observed with increasing NO_x mole fractions, for a fixed p_C. It appears to be due to the recent and moderately sensitive reaction (R17) 2 $HO_2 = 2$ OH + O_2 suggested by Klippenstein et al. [33]. Indeed, it increases the reactivity of pure H_2/air mixture although the sensitivity of this reaction decreases slightly with the addition of NO_x ($s_{R17} = 1.24$, 0.7, 0.5, 0.3 for $X_{NOx} = 0$, 50, 250, 1250 ppm, respectively), decreasing ignition delays. In addition, Fig. 7 displays a sensitivity analysis on the OH radical as a function of p_C, for a given composition ($X_{NOx} = 1250$ ppm). The competition between (R11), (R120), and (R4) is still observed and the sensitivity of (R120) decreases slightly when p_C increases ($s_{R120} = 2.1$, 1.2, 1, 0.9 for $p_C = 30$, 40, 50 and 60 bar, respectively. Alongside, the reaction (R17) shows a merely constant sensitivity with increasing p_C ($0.15 < s_{R17} < 0.2$). As a matter of fact, recently developed NO_x sub-mechanisms, including the one from Glarborg et al. [34] used in this study, were generally validated without taking into account (R17). Hence, the promoting effect of the NO/NO_2 recycling loop is combined with the promoting effect of (R17), explaining the shorter predicted ignition delays for the highest X_{NOx}. Noteworthily, the impact of (R17) on the other kinetic mechanisms predictions was also investigated, showing similar results. The ignition delays calculated with the Aljohani et al. including (R17) are available in the Supplementary Materials. Therefore, in light of this experimental and modelling study, it appears that NO_x sub-mechanisms need to be revisited considering (R17).

4. Conclusions

The main objective of this study was to measure ignition delay times for lean $H_2/O_2/N_2/NO_x$ mixtures under realistic hydrogen spark ignition engine conditions ($\varphi = 0.4$, $p_C = 30$ bar – 60 bar, and $T_C = 890$ K – 1000 K) and provide a reliable kinetic mechanism based on our previous work

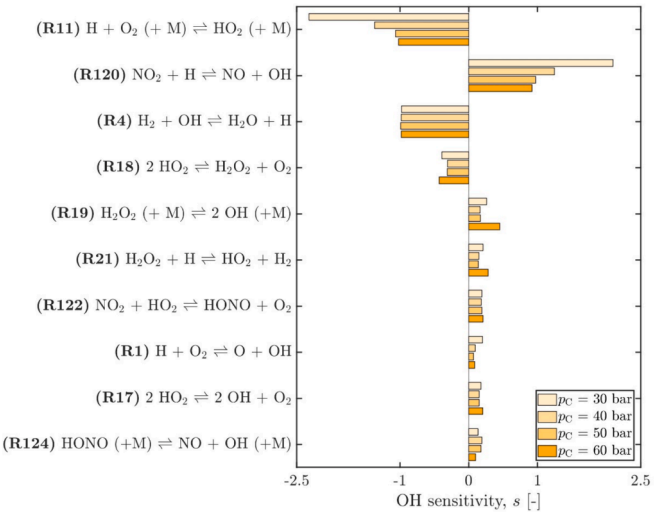

Fig. 7. Sensitivity on OH radical for H_2/air/NO_x mixtures for $X_{NOx} = 1250$ ppm, at $T_C = 920$ K, and $p_C = 30$ bar, 40 bar, 50 bar, 60 bar.

[31]. Four different mixtures were investigated with NO_x mole fractions of 0, 50 ppm, 250 ppm, and 1250 ppm. The interconversion of NO into NO_2 was simulated and experimentally quantified to account for the NO_x composition introduced in the chamber. Results indicate that ignition delay times decrease with NO_x addition, irrespective of the compression pressure. This highlights the importance of accurately predicting such combustion properties for modelling hydrogen internal combustion engines. Recent and optimized kinetic mechanisms were tested, notably our previously validated H_2/air kinetic mechanism [31] under similar conditions, completed with recent NO_x sub-chemistry. The proposed model displays very good agreement with experimental results. However, discrepancies appear for the highest NO_x concentrations. To understand the origins of these discrepancies and identify key reactions influencing the mixture reactivity enhancement, sensitivity analyses on the OH radical were performed. They reveal that the NO/NO_2 recycling loop combines with the HO_2/H_2O_2 pathway to increase the OH pool. In addition, the recent dismutation of HO_2 followed by the prompt dissociation of H_2O_2, namely 2 HO_2 = 2 OH + O_2, tends to promote the reactivity when the NO_x and the pressure increase, yielding an overprediction of the global reactivity. For future work, it is therefore crucial to focus the efforts on revisiting NO_x sub-mechanisms, taking into account this new reaction.

CRediT authorship contribution statement

N. Villenave: Writing – original draft, Software, Methodology, Investigation, Formal analysis, Data curation. **G. Dayma:** Writing – review & editing, Supervision, Formal analysis. **P. Brequigny:** Writing – review & editing, Supervision. **F. Foucher:** Writing – review & editing, Supervision, Conceptualization.

Declaration of competing interest

The authors declare that they have no known competing financial interests or personal relationships that could have appeared to influence the work reported in this paper.

Data availability

Supplementary data related to this article can be found in Supplementary Materials.

Acknowledgments

The support of the National Research Agency under grant number ANR-21-CE05-0004 (SPEEDYH ANR Project) is gratefully acknowledged. The authors are grateful for the support from Eng. B. Moreau and Dr. R. Oung from PRISME laboratory.

Appendix A. Supplementary data

Supplementary data to this article can be found online at https://doi.org/10.1016/j.fuel.2024.132482.

References

[1] International Energy Agency, Net Zero by 2050, https://www.iea.org/reports/net-zero-by-2050/, 2021; accessed September 2023.
[2] International Energy Agency, Global Energy Review: CO2 Emissions in 2021, https://www.iea.org/reports/global-energy-review-co2-emissions-in-2021-2/, 2022; accessed September 2023.
[3] International Energy Agency, Tracking Transport, https://www.iea.org/reports/tracking-transport-2021/, 2021; accessed September 2023.
[4] Teoh YH, How HG, Le TD, Nguyen HT, Loo DL, Rashid T, et al. A review on production and implementation of hydrogen as a green fuel in internal combustion engines. Fuel 2023;333:126525.
[5] Verhelst S, Wallner T. Hydrogen-fueled internal combustion engines. Prog Energy Comb Sci 2009;35:490–527.
[6] Verheslt S. Recent progress in the use of hydrogen as a fuel for internal combustion engines. Int J Hydrog Energ 2014;39:1071–85.
[7] Das LM. Hydrogen engines: a view of the past and a look into the future. Int J Hydrog Energ 1990;15:425–30.
[8] Law CK. Combustion physics. 1st Edition. Cambridge University Press; 2006.
[9] Rapp V, Killingsworth N, Therkelsen P, Evans R. Lean Combustion, Technology and Control – Lean-Burn Internal Combustion Engines. 2nd Edition,. Elsevier; 2016.
[10] Subramanian VJ, Mallikarjuna M, Ramesh A. Effect of water injection and spark timing on the nitric oxide emission and combustion parameters of a hydrogen fuelled spark ignition engine. Int J Hydrog Energ 2007;32:1159–73.
[11] Wan J, Zhuang Y, Huang Y, Qian Y, Qian L. A review of water injection application on spark-ignition engines. Fuel Process Technol 2021;221:106956.
[12] Dhyani V, Subramanian KA. Control of backfire and NOx emission reduction in a hydrogen fueled multi-cylinder spark ignition engine using cooled EGR and water injection strategies. Int J Hydrog Energ 2019;44:6287–98.
[13] A.M. Nande, S. Szwaja, J. Naber. (2008) Impact of EGR on Combustion Processes in a Hydrogen Fuelled SI Engine, SAE Technical Paper.
[14] Di H, He X, Zhang P, Wang Z, Wooldridge MS, Law CK, et al. Effects of buffer gas composition on low temperature ignition of iso-octane and n-heptane. Combust Flame 2014;161:2531–8.
[15] Song Y, He Y, Yu Y, Moreau B, Foucher F. Effect of exhaust gas recirculation and NO ignition delay times of iso-octane in a rapid compression machine. Energ Fuel 2020;34:8788–95.
[16] Sahu AB, Mohamed AAES, Panigrahy S, Saggese C, Patel V, Bourque G, et al. An experimental and kinetic modeling study of NOx sensitization on methane autoignition and oxidation. Combust Flame 2022;238:111746.
[17] Fuller ME, Morsch P, Preußker M, Goldsmith CF, Heufer KA. The impact of NOx addition on the ignition behaviour of n-pentane. React Chem Eng 2021;11:2191–203.
[18] Chen Z, Zhang P, Yang Y, Brear MJ, He X, Wang Z. Impact of nitric oxide (NO) on n-heptane autoignition in a rapid compression machine. Combust Flame 2017;186:94–104.
[19] Fang R, Saggese C, Wagnon SW, Sahu AB, Curran HJ, Pitz WJ, et al. Effect of nitric oxide and exhaust gases on gasoline surrogate autoignition: iso-octane experiments and modeling. Combust Flame 2022;236:111807.
[20] Song Y, He Y, Yu Y, Moreau B, Foucher F. Effect of exhaust gas recirculation and NO on ignition delay times of iso-octane in a rapid compression machine. Energ Fuels 2020;34:8788–95.
[21] Cai L, Ramalingam A, Minwegen H, Heufer KA, Pitsch H. Impact of exhaust gas recirculation on ignition delay times of gasoline fuel: an experimental and modeling study. Proc Comb Inst 2019;37:639–47.
[22] Cheng S, Saggese C, Goldsborough SS, Wagnon SW, Pitz WJ. Unraveling the role of EGR olefins at advanced combustion conditions in the presence of nitric oxide: ethylene, propene and isobutene. Combust Flame 2022;245:112344.
[23] M. Slack, A. Grillo, Investigation of hydrogen-air ignition sensitized by nitric oxide and by nitrogen dioxide, NASA-CR-2896 (1977).
[24] Mathieu O, Levacque A, Petersen EL. Effects of NO2 addition on hydrogen ignition behind reflected shock waves. Proc Comb Inst 2013;34:633–40.
[25] Pochet M, Dias V, Moreau B, Foucher F, Jeanmart H, Contino F. Experimental and numerical study, under LTC conditions, of ammonia ignition delay with and without hydrogen addition. Proc Comb Inst 2019;37:621–9.
[26] Goldsborough SS, Hochgreb S, Vanhove G, Wooldridge MS, Curran HJ, Sung CJ. Advances in rapid compression machine studies of low-and intermediate-temperature autoignition phenomena. Prog Energ Comb Sci 2017;63:1–78.
[27] Moffat RJ. Describing the uncertainties in experimental results. Fluid Sci: Exp. Therm; 1988.
[28] Baigmohammadi M, Patel V, Martinez S, Panigrahy S, Ramalingam A, Burke U, et al. Comprehensive experimental and simulation study of ignition delay time characteristics of single fuel C1–C2 hydrocarbons over a wide range of temperatures, pressures, equivalence ratios, and dilutions. Energ Fuel 2020;34:3755–71.
[29] ANSYS CHEMKIN 20.0, ANSYS Reaction Design 2020, (2020).
[30] T. Turànyi, Hydrogen for Future Thermal Engines – Reaction Kinetics of Hydrogen Combustion, 1st Edition (2023), Efstathios-Al. Tingas, Springer.
[31] Villenave N, Dayma G, Brequigny P, Foucher F. Experimental measurements of ultra-lean hydrogen ignition delays using a rapid compression machine under internal combustion engine conditions. Int J Hydrog Energ 2024;355:129431.
[32] Burke MP, Chaos M, Ju Y, Dryer FL, Klippenstein SJ. Comprehensive H2/O2 kinetic model for high-pressure combustion. Int J Chem Kinet 2012;44:7.
[33] Klippenstein SJ, Sivaramakrishnan R, Burke U, Somers KP, Curran HJ, Pitsch H, et al. HO2 + HO2: high level theory and the role of singlet channels. Combust Flame 2022:111975.
[34] Glarborg P, Miller JA, Ruscic B, Klippenstein SJ. Modelling nitrogen chemistry in combustion. Prog Energy Combust Sci 2018;67:31–68.
[35] Aljohani K, Mohamed AAES, Lu H, Curran HJ, Sarathy SM, et al. Impact of exhaust gas recirculation and nitric oxide on the autoignition of an oxygenated gasoline: experiments and kinetic modelling. Combust Flame 2024;259:113174.
[36] Sun W, Zhao Q, Curran HJ, Deng F, Zhao N, Zheng H, et al. Further insights into the core mechanism of h2/co/nox reaction system. Combust Flame 2022;245:112308.
[37] G.P. Smith, D.M. Golden, M. Frenklach, N.W. Moriarty, B. Eiteneer, M. Goldenberg, C.T. Bowman, R.K. Hanson, S. Song, W.C. Gardiner, V.V. Lissianski, Z. Qin http://www.me.berkeley.edu/gri_mech/, 2000.
[38] Sahu AB, Mohamed AAES, Panigrahy S, Saggese C, Patel V, et al. An experimental and kinetic modelling study of NOx sensitization on methane autoignition and oxidation. Combust Flame 2021;238:111746.

[39] Fang R, Saggese C, Wagnon SW, Sahu AB, Curran HJ, et al. Effect of nitroc oxide and exhaust gases on gasoline surrogate autoignition: iso-octane experiments and modelling. Combust Flame 2022;236:111807.
[40] N. Kawahara, U. Azimov. (2023) Hydrogen for Future Thermal Engines - Abnormal Combustion in Hydrogen-Fuelled IC Engines, 1st Edition, Efstathios-Al. Tingas, Springer.
[41] Li H, Karim GA. Knock in spark ignition hydrogen engines. Int J Hydrog Energy 2004;29:859–65.
[42] Ye Y, Gao W, Li Y, Zhang P, Gao X. Numerical study of the effect of injection timing on the knock combustion in a direct-injection hydrogen engine. Int J Hydrog Energy 2020;45:27919.
[43] Li Y, Gao W, Zhang P, Fu Z, Gao X. Influence of the equivalence ration on the knock and performance of a hydrogen direct injection internal combustion engine under different compression ratios. Int J Hydrog Energy 2021;46:11982–93.